

**SYNTHESIS AND CHARACTERIZATION OF  
CARBON NANOTUBE PREPARED USING  
MICROWAVE OVEN FOR HYDROGEN GAS  
SENSING APPLICATION**

**NATHEER ALI ALGADRI**

**UNIVERSITI SAINS MALAYSIA**

**2018**

**SYNTHESIS AND CHARACTERIZATION OF  
CARBON NANOTUBE PREPARED USING  
MICROWAVE OVEN FOR HYDROGEN GAS  
SENSING APPLICATION**

**by**

**NATHEER ALI ALGADRI**

**Thesis submitted in fulfillment of the requirements  
for the degree of  
Doctor of Philosophy**

**March 2018**

## ACKNOWLEDGEMENT

First and foremost, I would like to thank Allah for granting me health and patience to finish this research. I would also like to express my sincere gratitude to my main supervisor, **Prof. Dr. Zainuriah Hassan** for her valuable guidance and support throughout these study years. Without her comments and continuous encouragement, this dissertation would not have been possible. Thank you professor for having your door open every time I needed help. I consider myself very lucky and most honored to have been one of her students. I would also like to thank the my previous supervisor Prof. Dr. Kamarulazizi Ibrahim for his cooperation throughout this study.

My appreciation also goes to the staff of the Nano-Optoelectronics Research and Technology Laboratory (N.O.R Lab) and of Solid State laboratory for their technical assistance during my laboratory work.

My heartfelt gratitude also goes to my family members: to my mother and father, my wife and kids ,brothers and sisters for their continuous prayers, and endless support when I needed it.

Many thanks to my friend Ahmad diabat, and to all my friends and colleagues who supported and helped me at the School of Physics, University Sains Malaysia. Lastly, special thanks go to the professional editor, Dr. Mohammed Bououdina for his valuable academic comments and editing.

Natheer Algadri

March 2018

Penang, Malaysia

## TABLE OF CONTENTS

<b>ACKNOWLEDGEMENT</b>	<b>ii</b>
<b>TABLE OF CONTENTS</b>	<b>iii</b>
<b>LIST OF TABLES</b>	<b>viii</b>
<b>LIST OF FIGURES</b>	<b>ix</b>
<b>LIST OF SYMBOL</b>	<b>xvii</b>
<b>LIST OF ABBREVIATIONS</b>	<b>xix</b>
<b>ABSTRAK</b>	<b>xxii</b>
<b>ABSTRACT</b>	<b>xxiv</b>
<b>CHAPTER 1: INTRODUCTION</b>	<b>1</b>
1.1 Introduction	1
1.2 Problem statement	2
1.3 Research objectives	4
1.4 Originality of research	5
1.5 Thesis outline	6
<b>CHAPTER 2: LITERATURE REVIEW AND THEORETICAL BACKGROUND</b>	<b>7</b>
2.1 Introduction	7
2.2 Literature review for synthesis carbon nanotube	7
2.2.1 Introduction	7
2.2.2 Synthesis of carbon nanotube using microwave irradiation	8
2.2.2(a) Synthesis in gas phase	8
2.2.2(b) Synthesis in liquid phase	11
2.2.2(c) Solid precursor materials (Solid–Vapor–Solid Transformation)	12

2.3	Gas sensor based on CNT	18
2.4	Theoretical background	26
2.4.1	Structural properties of carbon nanotube	26
2.4.2	Hybridization	32
2.4.2(a)	$sp^3$ -hybridization	32
2.4.2(b)	$sp^2$ -hybridization	34
2.4.3	Rolled carbon materials	35
2.4.3(a)	Rehybridization	35
2.4.3(b)	Reactivity	35
2.4.4	Metal and semiconductor CNT	36
2.4.5	n-type and p-type carbon nanotube:	37
2.4.6	Microwave interactions with carbon materials	38
2.4.7	Growth mechanism of CNTs	42
2.4.8	Purification of carbon nanotubes	45
2.4.9(a)	Oxidation	45
2.4.9(b)	Ultrasonication	46
2.4.9(c)	Acid treatment	46
2.4.9(d)	Centrifugation	46
2.4.9	Oxidation mechanism	47
2.4.10	Dielectrophoresis (DEP) method	48
2.4.11	Raman spectroscopy	49
2.4.12	Metal-semiconductor contact	51
2.4.9(a)	Schottky contact	52

2.4.9(b) Ohmic contact	53
2.4.13 Operational parameter of gas sensor	54
2.4.10(a) Sensitivity	54
2.4.10(b) Recovery and response time	55
2.4.11(c) Gas sensor mechanism	56
<b>CHAPTER 3: METHODOLOGY AND EXPERIMENTAL PROCEDURE</b>	<b>58</b>
3.1 Introduction	58
3.2 Synthesis and characterization of CNTs using commercial microwave oven	59
3.2.1 Synthesis of CNTs using different ratio of graphite and ferrocene	59
3.2.2 Synthesis of CNTs using different diameters of ferrocene	60
3.3 Fabrication of gas sensor device based on carbon nanotube	60
3.3.1 Wet oxidation of silicon wafer	60
3.3.2 Carbon nanotube treatment	61
3.3.2(a) Magnetic stirring in HNO <sub>3</sub> acid	61
3.3.2(b) Ultrasonication process	61
3.3.2(c) Centrifugation process	62
3.3.2(d) Naturalizing processes	62
3.3.2(e) Drying processes	62
3.3.3 Metal contact deposition	63
3.3.4 Dielectrophoretic deposition method	63
3.4 Characterization instruments	65
3.4.1 Field emission scanning electron microscope (FESEM)	65
3.4.2 X-Ray diffraction method	66

3.4.3	Raman spectroscopy	68
3.4.4	Fourier transform infrared spectrometer (FTIR)	70
3.4.5	UV-Visible spectrophotometer	71
3.4.6	Transmission electron microscopy (TEM)	72
3.4.7	Gas sensor fabrication and testing system	73
3.4.8(a)	RF-sputtering system	73
3.4.8(c)	Gas Sensing Setup System	74
<b>CHAPTER 4: RESULTS AND DISCUSSION FOR CNT SYNTHESIZED USING MICROWAVE OVEN</b>		<b>76</b>
4.1	Introduction	76
4.2	Growth of carbon nanotube using different ratios of graphite and ferrocene	76
4.2.1	Raman spectroscopy analysis	76
4.2.2	FESEM and TEM observations	79
4.2.3	Optical properties	82
4.2.4	X-ray diffraction analysis	84
4.3	Growth of carbon nanotube using different ferrocene catalyst particle size	86
4.3.1	FESEM and TEM observations	86
4.3.2	X-ray diffraction analysis	89
4.3.3	Raman spectroscopy analysis	92
4.4	Functionalization and purification of CNT (F-CNT)	95
4.4.1	FESEM and EDX observation	95
4.4.2	Raman spectroscopy analysis	98
4.4.3	FTIR observation analysis	100
4.5	Summary	101

<b>CHAPTER 5: RESULTS AND DISCUSSION FOR H<sub>2</sub> GAS SENSORS BASED ON CNTS SYNTHESISED USING MICROWAVE OVEN</b>	<b>102</b>
5.1 Introduction	102
5.2 Carbon nanotube based hydrogen gas sensor fabricated on SiO <sub>2</sub> /Si substrate	102
5.3 Carbon nanotube based hydrogen gas sensor fabricated on glass substrate	111
5.3.1 Introduction	111
5.3.2 Hydrogen sensing characterization	111
5.3.3 Activation energy of the gas sensor	117
5.4 Effect of CNT treatment on H <sub>2</sub> gas sensor performance	118
5.5 Summary	123
<b>CHAPTER 6: CONCLUSION AND FUTURE WORK</b>	<b>124</b>
6.1 Conclusion	124
6.2 Future research studies	126
<b>REFERENCES</b>	<b>127</b>
<b>LIST OF PUBLICATIONS</b>	



## LIST OF TABLES

	<b>Page</b>
Table 2.1	Summary of the CNT synthesized using microwave method. 17
Table 2.2	Summary of various nanostructured materials produced using different synthesis technique. 25
Table 2.3	The properties of SWNT and MWNT. 32
Table 2.4	Penetration depth data of some materials and liquids for radiation at 2.45 GH. 42
Table 4.1	Comparison of Raman bands intensities for CNTs produced using graphite/ferrocene mixture ratios. 78
Table 4.2	Summery of XRD analysis for the grown CNT using different ratio of graphite/ferrocene. 86
Table 4.3	XRD parameters of CNTs as function of ferrocene catalyst particle size. 91
Table 4.4	Raman spectroscopy structural parameters of CNTs as function of ferrocene catalyst particle size. 94
Table 4.5	EDX analysis of as-prepared CNT and treated CNT using HNO <sub>3</sub> acid. 96
Table 4.6	Comparison of Raman bands intensities and FWHM G for R-CNTs and F-CNT. 98
Table 5.1	The comparison of the gas sensing parameters of the CNT based gas sensor on SiO <sub>2</sub> /Si substrate at different operating temperatures. 110
Table 5.2	Comparison of H <sub>2</sub> sensing properties between the present work and CNTs and other materials based sensors under different H <sub>2</sub> concentrations and temperatures reported in the literature. 116
Table 5.3	Comparison of the sensing properties to 300 ppm of H <sub>2</sub> gas between R-CNT (figure 5.15) and F-CNT (figure 5.13) at a temperature 75 °C. 122

## LIST OF FIGURES

	<b>Page</b>
Figure 2.1      A domestic MW oven with a quartz reactor and a catalyst-coated substrate [23].	9
Figure 2.2      A set-up including a commercial single-mode microwave reactor and liquid carbon sources for the synthesis of CNTs on catalyst-coated substrates [25].	10
Figure 2.3      a) Schematic illustration of the microwave-assisted synthesis of a self-assembled 3D G–CNT–Ni nanostructure. SEM images of (b) a wavy reduced graphene oxide sheet obtained by thermal exfoliation (c) well-distributed nickel nanoparticles on the inner and outer surfaces of graphene, which catalyze the CNT growth between graphene layers and (d) full-grown CNTs after completion of the MW irradiation [26].	11
Figure 2.4      Material obtained in an evacuated ampoule directly exposed to microwaves for 10 min: a) SEM image at low magnification of parallel arrays of aligned MWNTs; b) higher magnification of the rectangular of a MWNT zone marked in (a), and (c) TEM of metal particle at the tip [28].	12
Figure 2.5      (a) Microwave irradiation system. Morphology of the ACF specimen (b) before microwave irradiation, (c) after microwave irradiation. (d) Magnified image of (b) [29].	13
Figure 2.6      (a) Setup for synthesis of carbon nanotubes by using a remodeled domestic microwave oven and an Art Box, (b)TEM images of the products calcined at 800 °C and (c) Raman spectra of the carbon products at 600 °C, 700 °C, 800 °C and 900 °C for 5, 10, 15 and 20 min [31].	15
Figure 2.7      (a) Schematic illustration of CNT-fabrication processes utilizing solid precursors and additional susceptor materials, (b) Pop-tube approach applying a conducting polymer as MW susceptor to grow CNTs	

	on engineering materials (b) FESEM images of the resulting (a) [8]. (c) Microwave synthesis triggered by a single carbon fiber vertically placed to ferrocene precursor powder resulting in MWCNTs and (d) TEM images of the resulting (c) [34].	16
Figure 2.8	SEM images and a photograph of (a) spin-capable CNTs showing alignment of 430 $\mu\text{m}$ MWCNTs, (b) morphology of the CNT sheets, (c and d) CNTs sheet pulling from the CNT forest, , (e) Sensitivity and (f) cyclic response of the gas sensor after thermal annealing with 2000 sccm of $\text{N}_2$ [39].	19
Figure 2.9	(a) Schematic diagram of fabricated device and (b) SEM image of fabricated interdigitated electrodes and (c) Sensor sensitivity of P-MWCNTs and F-MWCNTs film at different concentrations of $\text{H}_2$ [40].	20
Figure 2.10	Resistive hydrogen sensors. (a) Metal-electrode CNT sensor, and (b) CNT-supported Pd film sensor. (c) Response of the Pd-electrode CNT sensor at medium $\text{H}_2$ concentrations and (d) Response of the CNT-supported Pd film sensor at medium $\text{H}_2$ concentrations [44].	22
Figure 2.11	(a) Photograph of a gas sensor device, wired for testing. SWCNT films were 3 mm wide, and 6 mm long between source and drain pads. (b) Images of nominally 7 nm films with sputtered Pd (AFM, scale in nm). (c) Fractional change in resistance as a function of $\text{H}_2$ concentration in $\text{N}_2$ , the resistance was taken 5 min after exposure to the $\text{H}_2$ -containing ambient. (d) $\Delta R/R$ as a function of time for exposure and recovery to the $\text{H}_2$ concentrations for 7 nm SWCNT films coated with sputtered Pd, recovery in $\text{N}_2$ [45].	23
Figure 2.12	(a) Scanning electron micrograph of ZnO multiple nanorods and (b) relative response of Pd-coated nanorods as a function of $\text{H}_2$ concentration in $\text{N}_2$ [47].	24
Figure 2.13	Allotropes of carbon. (a) Diamond. (b) Graphite. (c) Amorphous carbon. (d) Spherical fullerene, $\text{C}_{60}$ . (e) Ellipsoidal fullerene, $\text{C}_{70}$ . (f) Tubular fullerene,	

	SWCNT. The carbon atoms are in a tubular formation [70].	27
Figure 2.14	Basic structures of (a) single-walled, (b) double-walled, and (c) multi-walled CNTs [72].	28
Figure 2.15	The 2D graphene sheet diagram showing a vector structure classification used to define CNT structure [75].	29
Figure 2.16	Molecular models of exhibited by SWNTs based on the chirality: (a) armchair, (b) zigzag, and (c) chiral based conformation [82].	31
Figure 2.17	$sp^3$ -hybrid orbital [84].	33
Figure 2.18	(a) $sp^2$ -hybrid orbital. (b) Crystal structure of graphite [84].	34
Figure 2.19	(a) Microwave radiation properties in the traditional microwave oven. (b) Comparison of microwave heating versus conventional heating [106].	39
Figure 2.20	Diagram of the microwave field distribution in (a) a monomode reactor and (b) a common multimode parallel synthesis reactor [105].	40
Figure 2.21	Schematic diagram which demonstrates the possible growth mechanism of CNTs synthesized by the MW oven: (I) formation of catalyst particle; (II) dissolution and precipitation of C and nucleation of CNT with or without formation of graphitic cap; (III) a small part of the catalyst particle is drawn and lifted up with growing CNT; (IV) continuation of CNT growth: migration and attachment of Fe atoms/small particles to the catalyst particle; (V) repetition of the sequence of processes from (II) to (IV) [121].	44
Figure 2.22	Scheme for modification of CNTs with COOH group [133].	47
Figure 2.23	Particle polarization and DEP forces under positive and negative DEP [138].	49

Figure 2.24	Energy band diagram of perfect metal and n-type semiconductor Schottky contact under thermal equilibrium (a) before contact and (b) after contact [145].	52
Figure 2.25	Energy band diagram of perfect metal and n-type semiconductor ohmic contact under thermal equilibrium (a) before contact and (b) after contact [145].	54
Figure 2.26	The recovery and response times for a gas sensor.	55
Figure 3.1	Schematic of the methodology.	58
Figure 3.2	Schematic illustration of CNTs fabrication from a powder mix of ferrocene and graphite.	59
Figure 3.3	Schematic illustration of CNTs growth from Fe nanoclusters of different diameter sizes.	60
Figure 3.4	CNT treatment steps.	62
Figure 3.5	Schematic diagram of CNT gas sensor fabrication using DEP.	64
Figure 3.6	Micro-image of the as-fabricated metallic electrode (a) on glass substrate and (b) on SiO <sub>2</sub> /Si substrate.	65
Figure 3.7	The schematic diagram and the image of Field emission scanning electron microscope FESEM system (FEI Nova NanoSEM 450) [155].	66
Figure 3.8	Bragg diffraction in a crystal. The angles at which diffraction occurs are a function of the distance between planes and the X-ray wavelength [156].	66
Figure 3.9	Scheme of the possible occurring Raman processes [159].	69
Figure 3.10	Raman spectroscopy system (Renishaw inVia Raman microscope)[160].	70
Figure 3.11	Schematic optical diagram of a Fourier-transform infrared (FTIR) spectrometer [161].	70

Figure 3.12	The Cary 5000 is a high-performance UV-Vis-NIR spectrophotometer with its schematic diagram [162].	71
Figure 3.13	A schematic illustration of Transmission electron microscopy (TEM) [163].	72
Figure 3.14	Schematic diagram of an RF magnetron sputtering system [164].	73
Figure 3.15	H <sub>2</sub> gas sensor system.	74
Figure 4.1	Raman spectra recorded in the region 1000-3000 cm <sup>-1</sup> for CNTs synthesized by microwave irradiation for graphite/ferrocene mixture powder ratios (a) 80:20 (b) 70:30 (c) 50:50 (d) 60:40.	78
Figure 4.2	(a) Raman spectra obtained in the region between 1100 and 1900 cm <sup>-1</sup> for CNTs synthesized by MW irradiation for ratio 70:30 (b) Raman spectra of CNTs display optical phonon mode G-band at ~1580 cm <sup>-1</sup> . Lorentzian fitting (color lines) shows three component.	79
Figure 4.3	FESEM images of the CNTs synthesized using microwave oven after 5 s of irradiation of graphite/ferrocene mixture ratios of (a) 80:20, (b) 70:30, (c) 50:50, (d) 40:60.	80
Figure 4.4	TEM image of CNT synthesized by microwave irradiation from graphite/ferrocene mixture powder ratio of 70:30.	81
Figure 4.5	UV–Vis absorption spectra of CNTs suspensions in aqueous SDS synthesized by microwave irradiation from different graphite/ferrocene ratios.	82
Figure 4.6	Plot of absorbance against CNTs concentration synthesized using graphite/ferrocene mixture ratios of 80:20, 70:30, 50:50 and 40:60.	83
Figure 4.7	Jars containing CNTs suspended in aqueous SDS at different graphite/ferrocene ratios.	84

Figure 4.8	X-ray diffraction pattern of CNTs powder synthesized from graphite/ferrocene mixture powder ratio of 80:20, 70:30, 50:50 and 60:40.	85
Figure 4.9	Microscope images of ferrocene catalysts particle size (a) 27.0 $\mu\text{m}$ (b) 23.6 $\mu\text{m}$ , (c) 21.4 $\mu\text{m}$ and (d) 19.7 $\mu\text{m}$ . The inset represents histograms of catalyst particle size plotted as solid lines corresponding to a Gaussian fit.	87
Figure 4.10	FESEM images of CNTs grown using various ferrocene catalysts particle size: (a) 27.0 $\mu\text{m}$ , (b) 23.6 $\mu\text{m}$ , (c) 21.4 $\mu\text{m}$ , (d) 19.7 $\mu\text{m}$ . The inset represents histogram of catalyst particle size plotted as solid lines corresponding to a Gaussian fit.	88
Figure 4.11	High resolution FESEM images of CNTs grown using various ferrocene catalysts particle size: (a) 27 $\mu\text{m}$ , (b) 23.6 $\mu\text{m}$ , (c) 21.4 $\mu\text{m}$ , (d) 19.7 $\mu\text{m}$ . The inset show TEM images of selected CNT (the scale bar is 100 nm).	89
Figure 4.12	(a) XRD patterns of CNTs grown using various ferrocene catalysts particle size: 27.0 $\mu\text{m}$ (sample 1), 23.6 $\mu\text{m}$ (sample 2), 21.4 $\mu\text{m}$ (sample 3), 19.7 $\mu\text{m}$ (sample 4) and (b) zoom of XRD patterns in the region $25.5^\circ - 27.5^\circ$ .	90
Figure 4.13	(b) Evolution of FWHM for 002 peak as a function of CNTs average diameter (a) variation of $d_{(200)}$ spacing, calculated from the position of (002) reflection and (solid lines indicate linear fit).	91
Figure 4.14	Raman spectra of CNTs grown using various ferrocene catalysts particle size: 27 $\mu\text{m}$ (sample 1), 23.6 $\mu\text{m}$ (sample 2), 21.4 $\mu\text{m}$ (sample 3) and 19.7 $\mu\text{m}$ (sample 4).	93
Figure 4.15	Evolution of FWHM for (a) D, (b) G, and (c) 2D bands (solid lines indicate linear fit) and (d) evolution of the relative intensities $I_D/I_G$ , as function of CNTs average diameter (solid lines indicate the trend).	94
Figure 4.16	SEM images for (a) and (c) as-prepared CNT (b) and (d) $\text{HNO}_3$ treated CNT.	97

Figure 4.17	(a) and (c) EDX analysis of acid treatment CNT and as-prepared CNT, (b) and (d) FESEM of acid treatment CNT and as-prepared CNT.	97
Figure 4.18	The Raman spectra of “as-prepared” (R-CNT) and functionalized carbon nanotube (F-CNT).	99
Figure 4.19	The FTIR spectra of “as-prepared” (R-CNT) and functionalized carbon nanotube (F-CNT).	100
Figure 5.1	Cross section FESEM micrographs of SiO <sub>2</sub> layer.	103
Figure 5.2	The current–voltage characteristics of F-CNT based gas sensor without H <sub>2</sub> at room temperature.	103
Figure 5.3	Sensitivity and repeatability of CNTs-based gas sensor under exposure to a dilute H <sub>2</sub> atmosphere (140 ppm) at different temperature (a) RT, (b) 50 °C, (c) 75 °C and (d) 100 °C.	104
Figure 5.4	Sensitivity of CNTs-based gas sensor under exposure to a dilute H <sub>2</sub> gas with different concentrations (20 to 140 ppm) at different temperatures (a) room temperatures (b) 50 °C, (c) 75 °C (d) 100 °C.	106
Figure 5.5	Variation of sensitivity measured for CNT based gas sensor upon exposure to dilute H <sub>2</sub> atmosphere with different operating temperature.	107
Figure 5.6	(a) Variation of the sensitivity with operating temperature for CNTs/ H <sub>2</sub> gas sensor and (b) variations in response and recovery time with temperature.	108
Figure 5.7	The Sensitivity and cyclic response of the CNTs based gas sensor under exposure to a dilute H <sub>2</sub> atmosphere (1000 ppm) at different temperatures (a) RT, (b) 50 °C, (c) 75 °C and (d) 100 °C.	112
Figure 5.8	Sensitivity of the CNT based gas sensor under exposure to a dilute H <sub>2</sub> gas with different concentrations (20 to 1000 ppm) at different temperatures (a) room temperature (b) 50 °C, (c) 75 °C and (d) 100 °C.	113



Figure 5.9	(a) Change of sensitivity measured for CNT based gas sensor upon exposure to dilute H <sub>2</sub> atmosphere with different operating temperature. (b) The variation of the sensitivity with operating temperature for MWCNTs H <sub>2</sub> gas sensor.	115
Figure 5.10	Arrhenius plot of $\ln(dI/dt)$ versus reciprocal operating temperature ( $1/T$ ).	118
Figure 5.11	Changes in the response of F-CNT gas sensor upon exposure to different concentrations (20-300 ppm) of H <sub>2</sub> gas at room temperature. The inset shows the response of CNT gas sensor during the time 0-10 s.	119
Figure 5.12	Changes in the response of F-CNT gas sensor upon exposure to different concentrations (20-300 ppm) of H <sub>2</sub> gas at temperature 50 °C.	119
Figure 5.13	Changes in the response of F-CNT gas sensor upon exposure to different concentrations (20-300 ppm) of H <sub>2</sub> gas at temperature and 75 °C.	120
Figure 5.14	The plot of the maximum responses measured from the switching On/Off H <sub>2</sub> gas every 2 min for 10 cycles summarized from F-CNT/R-CNT based gas sensors upon exposure concentrations (20–300 ppm) at different operating temperatures.	121
Figure 5.15	Changes in the response of R-CNT gas sensor upon exposure to different concentrations (20-300 ppm) of H <sub>2</sub> gas at temperature 75 °C.	122
Figure 5.16	Schematic representation the sites for adsorption of H <sub>2</sub> gas molecules.	123

## LIST OF SYMBOL

$T$	Absolute temperature
$E_a$	Activation energy
$\phi_B$	Barrier hight
$K_B$	Boltzmann's constant
$^{\circ}\text{C}$	Celsius temperature
$e$	Charge of electron
$I$	Current
$I_{\text{air}}$	Current in the presence of air ambience
$I_{\text{gas}}$	Current in the presence of gas ambience
$\theta$	Diffraction angle
$\gamma_d$	Domain size broadening
$\chi_s$	Electron affinity of semiconductor
$\text{eV}$	Electron volte
$E_g$	Energy bandgap
$E_F$	Fermi level
$\nu$	Frequency
$\text{Hz}$	Hertz
$\text{HCl}$	Hydrochloric acid
$\text{HF}$	Hydrogen fluoride
$\text{H}_2\text{O}_2$	Hydrogen peroxide

OH	Hydroxyl group
$I_D$	Intensity of D band in Raman
$I_G$	Intensity of G band in Raman
d	Interplanar spacing
M	Molarity
$D_p$	Penetration depth
h	Planck's constant
k	Rate of the current change
R	Resistance
S	Sensitivity
SiO <sub>2</sub>	Silicon dioxide
$\gamma_f$	Strain broadening
H <sub>2</sub> SO <sub>4</sub>	Sulfuric acid
V	Voltage
W	Watt
$\lambda$	Wavelength
$\phi$	Work function

## LIST OF ABBREVIATIONS

ACF	Activated carbon fibre
Amp	Ampere
AAO	Andic aluminium oxide
R-CNT	As-produced carbon nanotube
ADC	Azodicarbonamide
a <sub>c-c</sub>	Carbon -carbon bond length
CNT	Carbon nanotube
CPD	Chemical path deposition
CVD	Chemical vapour deposition
Con.	Concentration
D <sub>2</sub> O	Deionised water
DEP	Dielectrophoretic
EDX	Energy dispersive X-ray spectroscopy
Fr	Ferrocene
FET	Field effect transistor
FESEM	Field emission scanning electron microscopy
FWHM	Full width half maximum
F-CNT	Functionalization carbon nanotube
Gr	Graphite
HR-XRD	High resolution X-ray diffraction

IDE	Interdigital electrodes
LAR	Laser assisted reaction
MS	Metal - semiconductor
MACE	Metal assisted chemical etching
ME	Metal electrode
MSM	Metal-semiconductor-metal
$\mu$ W	Micro-watt
MW	Microwave
MCNT	Multi wall carbon nanotube
NBE	Near-band edge emission
NIR	Near-infrared
n-type	Negative type
1D	One-dimensional
ppm	Part per million
PE	polyethylene
PET	Polyethylene terephthalate
PPy	Polypyrrole
p-type	Positive type
PLV	Pulse laser vaporization
RF	Radio frequency
RT	Room temperature
rms	Root mean square

rpm	Round per minute
SE	Secondary electrons
SCNP	Shell shaped carbon nanoparticle
SWNT	Single wall carbon nanotube
SDS	Sodium dodecyl sulphate
Sccm	Standard cubic centimetres per minute
TErGO	Thermally exfoliated reduced graphite oxide
TEM	Transmission electron microscopy
2D	Two-dimensional
UV	Ultraviolet
VLS	Vapor-liquid-solid
VS	Vapor-solid
Vis	Visible

**SINTESIS DAN PENCIRIAN NANOTIUB KARBON YANG  
DISEDIAKAN DENGAN MENGGUNAKAN KETUHAR GELOMBANG  
MIKRO BAGI APLIKASI PENDERIAAN GAS HIDROGEN**

**ABSTRAK**

Nanotub karbon (CNTs) telah memperoleh perhatian yang besar kerana ciri-ciri elektrik, mekanikal, terma, kimia dan magnet yang tersendiri. Walau bagaimanapun, keperluan untuk kebanyakan kaedah sintesis sedia ada termasuk suhu tinggi atau persekitaran vakum yang tinggi. Oleh itu, terdapat keperluan untuk kaedah yang lebih mudah dan rendah untuk mensintesis CNT. Kajian ini mencirikan sifat morfologi dan optik CNTs yang disintesis menggunakan ketuhar gelombang mikro. Penderia gas hidrogen yang berasaskan CNT kemudiannya difabrikasikan pada silikon oksida dan substrat kaca menggunakan kaedah pemendapan yang mudah dan kos efektif. Sintesis CNT melibatkan perataan campuran grafit dan pemangkin ferrosena di dalam ketuhar gelombang mikro di bawah keadaan ambien selama tempoh 5 s. Asid  $\text{HNO}_3$  digunakan untuk memfungsikan nanotub dan mengeluarkan zarah metalik. CNT yang disintesis diukur dan dicirikan oleh mikroskop imbasan elektron pancaran medan (FESEM), spektroskopi serakan tenaga X-ray (EDX), mikroskop penghantaran elektron (TEM), belauan sinar-X (XRD), spektroskopi Raman, spektroskopi ultraungu (UV) dan spektroskopi jelmaan Fourier inframerah (FTIR). CNT disintesis di bawah nisbah grafit dan ferrosena yang berbeza dan keputusan terbaik didapati pada nisbah 70:30 (grafit pada ferrosena). Pengaruh saiz zarah pemangkin pada pembentukan dan diameter CNT juga disiasat. Pemangkin ferrosena dengan diameter purata 19.7, 21.4, 23.6 dan 27.0  $\mu\text{m}$  digunakan. Spektroskopi Raman menunjukkan bahawa lebar penuh pada separuh maksimum (FWHM) dari jalur-jalur G, D, dan 2D berkurangan secara beransur-ansur dengan diameter CNT yang semakin meningkat. Sementara itu, nisbah

keamatan jalur-G/jalur-D didapati peka terhadap kecacatan hablur, menunjukkan penurunan untuk diameter CNT dalam lingkungan 25-40 nm, diikuti dengan sedikit peningkatan untuk diameter yang lebih tinggi. Ini mungkin dikaitkan dengan kelengkungan CNT dan ketegangan yang dibentuk di sepanjang dinding tiub. Analisis belauan sinar-X menunjukkan peningkatan dalam jarak antara lapisan  $d_{002}$  dengan pengurangan diameter CNT. Di samping itu, diameter CNT didapati berkadar songsang dengan lebar garis (002). Untuk mengfabrikasikan penderia gas, teknik elektroforetik digunakan untuk memendapkan nanotiub pada elektrod paladium. Penderia gas berasaskan CNT yang dirawat menunjukkan keupayaan baru dalam mengesan kepekatan  $H_2$  pada julat yang luas (20 hingga 1000 ppm) pada suhu bilik serta suhu operasi lain (50 hingga 100 °C). Di samping itu, penderia ini menunjukkan sifat penderiaan yang sangat baik seperti masa tindak balas/pemulihan yang singkat (89/19 s) dan kepekaan yang sangat tinggi (460%). Penderia gas hidrogen berasaskan CNT juga diasas, sebelum dan selepas rawatan  $HNO_3$ . Penderia yang dirawat didapati mempunyai kepekaan yang lebih tinggi dan masa tindak balas/pemulihan yang lebih pendek berbanding dengan CNT yang tidak dirawat. Kajian ini memberikan butiran mengenai ciri-ciri CNT yang disintesis dan aplikasinya dalam pembuatan penderia gas hidrogen dengan keupayaan penderiaan yang sangat baik pada suhu bilik.



**SYNTHESIS AND CHARACTERIZATION OF CARBON NANOTUBE  
PREPARED USING MICROWAVE OVEN FOR HYDROGEN GAS  
SENSING APPLICATION**

**ABSTRACT**

Carbon nanotubes (CNTs) have garnered substantial interest because of their distinctive electrical, mechanical, thermal, chemical and magnetic properties. However, the requirements for majority of the existing synthesis methods include high temperature or a high vacuum environment. Thus, there is the need for a simpler and low cost method for synthesizing CNT. This study characterizes the morphology and optical properties of CNTs synthesized using microwave oven. CNT based hydrogen gas sensors were then fabricated on silicon oxide and glass substrates using a simple and cost-effective deposition method. The synthesis of CNT entailed flattening a mixture of graphite and ferrocene catalyst inside the microwave oven under ambient conditions for 5 s duration.  $\text{HNO}_3$  acid was used to functionalize the nanotube and remove metallic particles. The synthesized CNTs were measured and characterized by field emission scanning electron microscopy (FESEM), energy dispersive X-ray Spectroscopy (EDX), transmission electron microscopy (TEM), X-ray diffraction (XRD), Raman spectroscopy, ultraviolet (UV) spectroscopy and Fourier transform infrared spectroscopy (FTIR). CNT was synthesized under different ratio of graphite and ferrocene the best results were found at ratio of 70:30 (graphite to ferrocene). The influence of catalyst particle size on the formation and diameter of CNTs was also investigated. Ferrocene catalysts with average diameters of 19.7, 21.4, 23.6 and 27.0  $\mu\text{m}$  were used. Raman spectroscopy indicates that the full width at half maximum (FWHM) of G, D, and 2D bands decreases gradually with increasing CNT diameter. Meanwhile, G-band/D-band intensity ratio is found to be sensitive to crystal defects,

showing a drop for CNTs diameter in the range of 25-40 nm, followed by a slight increase for higher diameters. This may be associated with CNTs curvature and strain which developed along tube walls. X-ray diffraction analysis demonstrates an increase in  $d_{002}$  interlayer spacing with decreasing CNT diameter. Furthermore, CNT diameter is found to be inversely proportional to full width half maximum of (002) reflection. In order to fabricate gas sensor, the electrophoretic technique was employed to deposit the nanotube on palladium electrode. The gas sensor based on treated CNT showed novel capability in detecting a broad range of  $H_2$  concentration (20 to 1000 ppm) at room temperature as well as other operating temperatures (50 to 100 °C). Additionally, this sensor demonstrated excellent sensing properties such as short response/recovery time (89/19 s) and very high sensitivity (460%). The CNT based hydrogen gas sensor was also investigated, before and after  $HNO_3$  treatment. The treated sensor was found to have higher sensitivity and shorter response/recovery time as compared to the nontreated CNT. This study provides details on the characteristics of synthesized CNT and its applicability in the manufacture of hydrogen gas sensors with excellent sensing capabilities at room temperature.

## CHAPTER 1: INTRODUCTION

### 1.1 Introduction

In order to develop new technologies, several science disciplines have made the search for new cutting-edge materials a focal point. In recent years, enormous interest has been devoted to the production of nanostructured materials such as nanotubes, nanoparticles or nanowires from various chemical reactions. In particular, carbon nanotubes (CNTs) have garnered substantial interest because of their distinctive electrical, mechanical, thermal, chemical and magnetic properties [1]. Mechanically, CNTs are very strong because of their relatively high elastic modulus ( $>1$  TPa) and tensile strength (63 GPa). CNTs also have superior electric and thermal properties. CNT can either be metallic or a semiconducting material, with maximum current density of  $\sim 10^{13}$  A/cm<sup>2</sup>, current capacity that is 1000 times greater than copper wires, thermal conductivity of 3000 W/mK and stability of up to 2800 °C in vacuum [2-4].

CNTs consist of two groups: single-wall carbon nanotubes (SWCNTs) and multi-wall carbon nanotubes (MWCNTs). Single-wall carbon nanotubes (SWCNTs) are rolled up structure of a single graphite layer, with diameter of about 1-2 nm, whereas, multi-wall carbon nanotubes (MWCNTs) are concentric graphite layers rolled up into a layer-layer structure with interlayer spacings of 0.34 nm and diameter range of 15-70 nm [5].

To obtain CNTs with desired properties, several techniques for the growth of CNTs have been adopted. The most commonly used methods include chemical vapor deposition, arc-discharge and laser ablation [6]. In addition, the microwave oven method is frequently used because it is a cost effective and facile technique for the

synthesis of CNTs at room temperature and ambient pressure. Unlike the other methods, the microwave oven method is simple to apply and a very fast technique [7, 8].

Semiconductor gas sensors (such as ZnO, SnO<sub>2</sub>, GaN) are generating tremendous interest due to their applications in industry, environmental monitoring, space exploration, biomedicine, and pharmaceuticals. Basic standards for these functional gas-sensing devices are highly sensitive, fast response time and recovery time, low power consumption, low operating temperature and high stability.

Recently, CNT-based gas sensors have attracted considerable attention due to their exceptional features, such as higher sensitivity, low operating temperature, and fast response stemming from its high surface-to-volume ratio [9]. CNT is also a viable source material in the manufacture of hydrogen gas sensor, since it is capable of sensing hydrogen [10].

## **1.2 Problem statement**

The requirements for majority of the currently available synthesis methods (laser ablation, plasma enhanced chemical vapor deposition, arc discharge [6]) include high temperature or a high (sometimes very high) vacuum environment to operate. Hence, these methods are expensive and problematic to upscale. In recent times, microwave radiation has played a significant part as a thermal source in the synthesis of carbon nanotubes.

In order to meet the growing requirement generated by many emerging applications Carbon nanotube is produced widely using various techniques. Hence, the use of microwave radiation has played a vital part as a thermal source for the synthesis of

CNTs attributable to its significant advantages over conventional methods: the most prominent its ability to rapidly attain maximum temperature in a very short time. This is important because the synthesis of CNTs by means of conventional heating normally requires a long time, usually several hours. By using the microwave oven, production time can be reduced to within few seconds, which ultimately saves time and conserves energy.

The penetration depth is a key parameter for characterizing materials heated via MW irradiation. The penetration depth is inversely proportional to the loss factor, hence low loss factor indicates high penetration depth and quasi-transparency of the material to microwave radiation. Conversely, materials with high loss factor exhibit a low penetration depth. Thus, only their surface is efficiently heated. The microwaves irradiation are specifically absorbed in highly conductive materials due to strong interactions between the electric field of the microwaves and the free electrons of the material. However, the bulk of the radiation incident on those materials is reflected, and the penetration depth is merely some tens of nanometers or micrometers. In addition, the loss factor for carbon materials usually increases considerably with temperature, resulting in the decrease of the penetration depth in carbon [11-13]. As a result, synthesis of carbon nanotubes using microwave oven relatively takes a long time in the previous studies, moreover, a small portion of the raw materials used in carbon nanotube production will absorb microwave radiation.

The one-dimensional nanoscale structure of CNT has a large surface area to volume ratio, which is an advantage for maximizing the surface response. Moreover, the radius, which is comparable to the length, offer greater potential in sensing performance, compared to bulk, by showing sensitive changes upon exposure to gas molecules. CNTs have been intensively investigated for use in gas

sensing devices due to their unique physical and chemical properties. It has been proven that CNTs present the semiconducting property due to their unique chirality. The absorbing gas molecules can significantly change the conductivity of CNTs by withdrawing and donating electrons [14, 15]. This behavior forms the basis for applications of CNTs as chemical gas sensors. Moreover, the high surface to volume ratio of CNTs provides an advantage in sub-ppm level gas detection [16].

The majority of the applications based on carbon nanotube require pure material relatively with negligible amounts of metal residues. However, as-prepared CNTs using microwave oven generally incorporate lots of impurities, basically consisting of iron nanoparticles that were introduced to catalyze the synthesis, amorphous carbon, carbon nanoparticles and graphite enclosed in carbon nanotube walls. As a result, the gas sensors based on pristine CNTs have certain limitations, such as sometimes low sensitivity to analytes, lack of selectivity (irreversibility) or long recovery time (from several minutes to several hours). Therefore, to retain the excellent intrinsic properties and the optimal performance of CNTs in the gas sensors, high-purity CNTs are required.

### **1.3 Research objectives**

In order to synthesize carbon nanotubes using microwave oven at room temperature under ambient environment and in the absence of inert or feedstock gases, a mixture of graphite and ferrocene was employed as starting material. The main objectives of the study are:

1. To synthesize carbon nanotube using a conventional microwave oven within short time and characterize the morphology and optical properties of carbon nanotubes (CNT).

2. To obtain the optimal growth of CNT nanostructures by using low-cost microwave method and study the effect of various ratio of graphite and ferrocene, and different diameter of ferrocene on the structural, morphological, and optical properties.
3. To improve H<sub>2</sub> gas sensor performance, especially at room temperature as well as increase the sensitivity and stability by purified and functionalized the pristine carbon nanotubes and investigate the influence of CNT treatment on the performance of H<sub>2</sub> gas sensor.
4. To fabricate low power, highly sensitive, and fast response CNT-based H<sub>2</sub> gas sensor using simple, fast, and a low-cost fabrication method on SiO<sub>2</sub>/Si and glass substrates

#### **1.4 Originality of research**

The originality of this study involves the following points:

1. The synthesis of carbon nanotube in one step using the conventional microwave oven at short time in ambient environment and in the absence of inert or feedstock gases.
2. The particle size effect of ferrocene catalyst on the structural and morphological characteristics of carbon nanotubes grown by microwave oven.
3. The fabrication of gas sensor based on CNT with high capability to detect a low H<sub>2</sub> concentration (20 ppm) at room temperature with ultra-low power consumption of 0.6 nW.
4. The enhancement of performance of the carbon nanotube-based H<sub>2</sub> gas sensor through decreasing the impurity using HNO<sub>3</sub> acid oxidation and centrifugation.

## **1.5 Thesis outline**

This study comprises of six (6) chapters. Chapter 1 introduces the theme of the research along with problem statement, originality of the research and objectives. Chapter 2 reviews relevant studies on the synthesis of CNT and fabrication of gas sensors based on carbon nanotubes. This chapter also presents the theoretical background of purification, structural and gas sensing properties of CNT. Chapter 3 entails the morphological characterization of CNTs synthesized using commercial microwave oven, and the fabricated CNT based gas sensor device. Chapter 3 also describes the instruments used in this research. Chapter 4 presents results on the growth of carbon nanotubes using different ratios of graphite/ferrocene and different diameter sized ferrocene compounds. The chapter further explains the functionalization of CNT using  $\text{HNO}_3$  acid. Chapter 5 discusses the CNT based hydrogen gas sensor fabricated on  $\text{SiO}_2/\text{Si}$  and glass substrates. The chapter provides details on the effect of acid treatment on the fabricated sensor. Finally, Chapter 6 comprises the conclusions of the study and future works.



## **CHAPTER 2: LITERATURE REVIEW AND THEORETICAL BACKGROUND**

### **2.1 Introduction**

This chapter reviews the relevant and contemporary studies on microwave synthesized carbon nanotubes (CNT). The synthesis parameters that influence the crystalline quality and morphology of CNTs are reviewed. In addition, studies on the characterization of CNT-based gas sensor are discussed. To conclude, the growth mechanisms of CNTs synthesized using microwave oven are analyzed.

### **2.2 Literature review for synthesis carbon nanotube**

#### **2.2.1 Introduction**

Carbon nanotubes (CNTs) have garnered immense interest, due to their unique electrical, mechanical, thermal, chemical and magnetic properties [1]. Furthermore, CNTs have been recommended as a source material in the manufacture of several devices, such as nanoelectronics, fuel cells, sensors and solar cells. Iijima is the first scientist to discover CNTs, and reported the preparation of multi-wall carbon nanotubes ( $C_{60}$ ) using the arc evaporation process in 1991 [17]. Iijima et al. and Bethune et al., also described the growth method of single walled carbon nanotubes (SWNTs) in 1993 [18].

CNTs can be synthesized using several methods that include laser ablation, plasma-enhanced chemical vapor deposition, and arc discharge [6]. Each of these methods have a number of benefits and drawbacks, resulting in different growth outcomes. Thus, the synthesis of CNTs with specific properties requires the selection of a particular preparation method. However, majority of the presently used synthesis

methods involve either high temperature or a high (occasionally very high) vacuum environment, which are costly and problematic to upscale. On the other hand, a number of microwave assisted methods have also been developed as viable alternatives to the conventional techniques [19-21].

carbon nanotubes (CNTs) since its discovery have generated great interest among researchers to explore their unique electrical, physical, mechanical and chemical properties to develop high performance devices. Researchers have been exploring the potential of CNTs in a wide range of applications: nanoelectronics, sensors, field emission, displays, hydrogen storage, batteries, polymer matrix composites, nanoscale reactors and electrodes [22]. The electrical properties of CNTs are extremely sensitive to charge transfer and chemical doping effects by various molecules. When electron-withdrawing molecules (e.g.  $\text{NO}_2$ ,  $\text{O}_2$ ) or electron-donating molecules (e.g.  $\text{NH}_3$ ,  $\text{H}_2$ ) interact with the semiconducting CNTs, they will change the density of the main charge carriers in the ‘bulk’ of the nanotube, which changes the conductance of CNTs. This behavior forms the basis for applications of CNTs as electrical chemical gas sensors [16].

### **2.2.2 Synthesis of carbon nanotube using microwave irradiation**

#### **2.2.2(a) Synthesis in gas phase**

The synthesis of CNTs using a microwave irradiation mechanism was first reported in 2002 by Park et al., [19, 23]. The authors utilized a combination of acetylene and hydrogen flowing through the reactor of a conventional microwave oven (800 W) under irradiation time of 0.5 to 30 min (Figure 2.1). In this system, black carbon was used as a substrate to synthesize the CNTs on its surface. Sulfur was used

as an additive component to overcome the energy loss problem in the substrates. The sulfur plays an important role by reducing the melting point and dissolving the catalyst in the carbon nanotube growth. However, cracks were identified when  $\text{SiO}_2$  was alternatively used as a substrate. This distortion of the substrate's morphology is an indication of the local heating of catalyst particles.[19, 23]

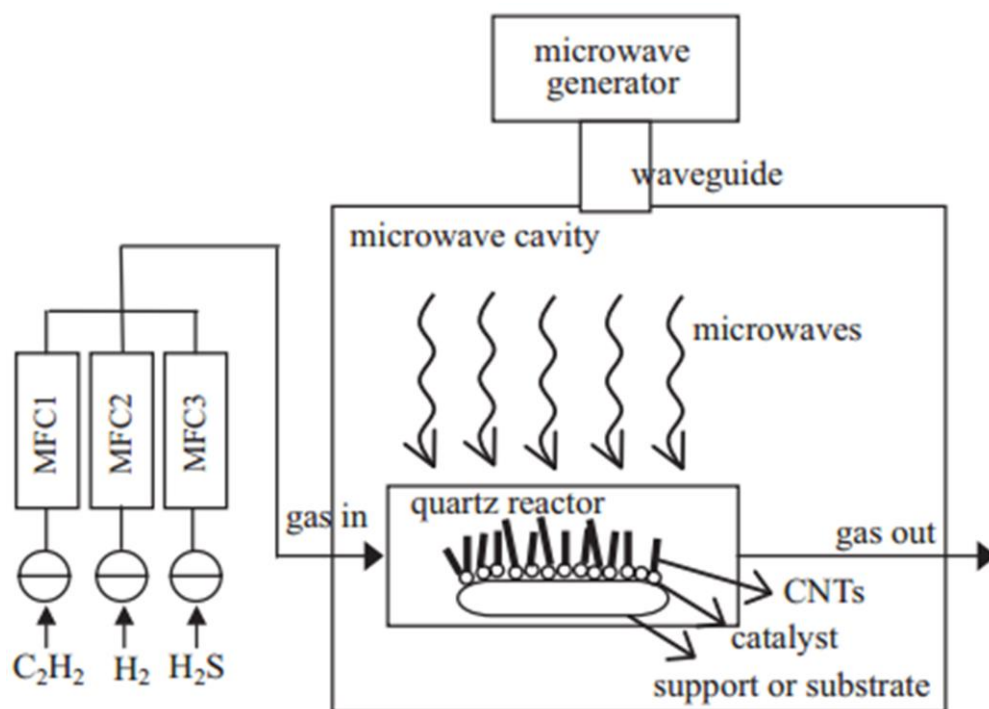


Figure 2.1: A domestic MW oven with a quartz reactor and a catalyst-coated substrate [23].

In a similar study, Fu et al. [24] employed the mixture of methane–nitrogen (1:4), to synthesize CNTs using a microwave oven with carbon felt as the microwave absorbing material and microwave power of 6 kW. The reaction was performed under flowing reactant gas at 1100 °C for 60 min, resulting in the formation of Y-shaped CNTs. The CNTs grow on a cluster of active carbon resulting from decomposition of methane during the microwave heating. The active carbon cluster acts as a nuclei for the carbon nanotube.

Druzhinina et al. [25] developed a reactor based on the conventional single-mode microwave to synthesize multi-wall CNTs on different substrates, such as quartz glass, silicon, and mica. CNTs have also been synthesized under microwave irradiation power of 300 for a duration of five minutes. Various catalysts have been utilized, which include nickel, iron and cobalt salts, and different alcohols as carbon sources. To date, the use of nickel and ethanol as catalyst material and carbon source, respectively, have provided the best results, as regards the symmetry and size of the CNTs synthesized using the microwave oven. Other optimum conditions for CNT synthesis include irradiation time of 5 min and microwave power of 200 W (Figure 2.2).

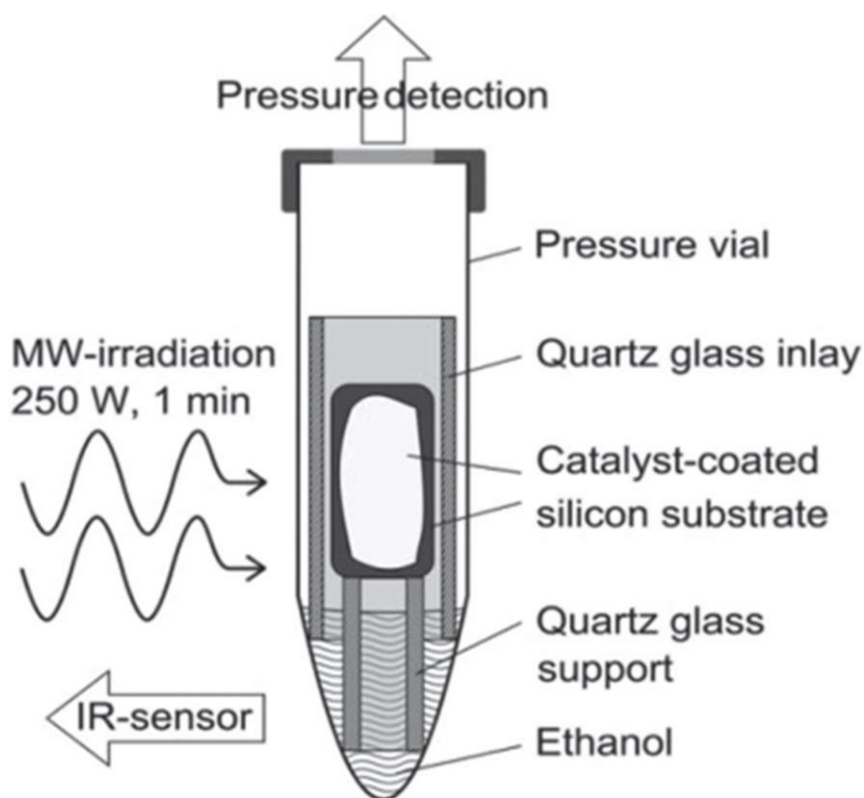


Figure 2.2: A set-up including a commercial single-mode microwave reactor and liquid carbon sources for the synthesis of CNTs on catalyst-coated substrates [25].

### 2.2.2(b) Synthesis in liquid phase

Oh et al., [26] used thermally exfoliated graphene oxide and nickelocene to synthesize CNTs directly on graphene sheets. The mixture was irradiated at 700 W inside a multimode MW oven for 5 min, then cooled for 5 min, after which the process was repeated a second time. The microwave treatment caused nickel nanoparticles to form on the graphene defects. The CNTs were subsequently developed on the nickel nanoparticles. A 3D graphene–CNT–nickel nanostructure was created because the nickel catalyst settle in the CNT tips (Figure 2.3). However, the study presented no detailed information on the ratio of the mixture, the obtained temperatures, and if the reaction mixture was agitated/stirred in the course of microwave irradiation.

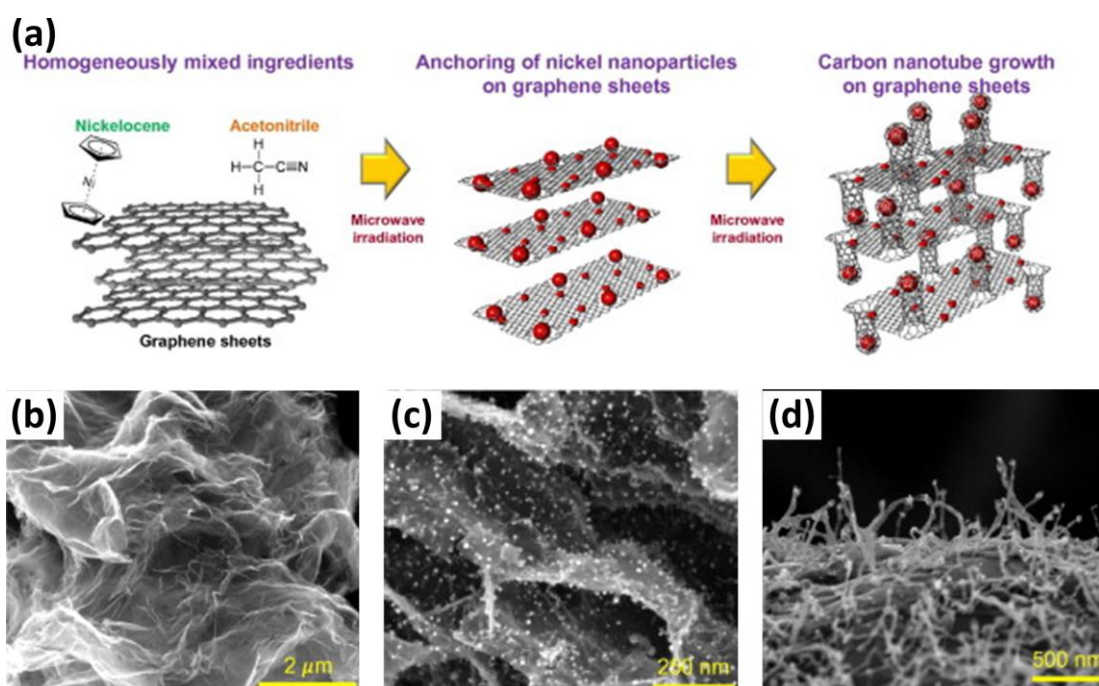


Figure 2.3: a) Schematic illustration of the microwave-assisted synthesis of a self-assembled 3D G–CNT–Ni nanostructure. SEM images of (b) a wavy reduced graphene oxide sheet obtained by thermal exfoliation (c) well-distributed nickel nanoparticles on the inner and outer surfaces of graphene, which catalyze the CNT growth between graphene layers and (d) full-grown CNTs after completion of the MW irradiation [26].

### 2.2.2(c) Solid precursor materials (Solid–Vapor–Solid Transformation)

Méndez et al. [27] synthesized CNTs via the vaporization of powdered graphite or mixtures of graphite with either sucrose or boric acid under vacuum, in the absence of a catalyst. The synthesis was carried out under a duration of 60 min (180 min for the boron compound) using a domestic microwave oven at 800 W. At oven temperature of approximately 1200 °C, CNTs were produced with diameters between 50 to 400 nm. In a similar study, Vivas-Castro et al. [28] synthesized multi-wall carbon nanotubes (MWCNTs) by mixing graphite with iron acetate in a quartz. The mixture was then irradiated using a commercial MW oven with a power of 1000 W and vacuum ambient (Figure 2.4). The ampoules were either subjected to direct irradiation or were partially submerged in water. In the submerged case, most of the microwave radiation was absorbed by the water, hence only weak irradiation reached the sample. Therefore, the temperature increased gradually and constantly. The boiling water then initiates the vibration of the ampoules. The entire graphite were converted into MWCNTs after 120 min. Conversely, 7 min was sufficient to synthesize MWCNTs without water. However, the absence of water caused the temperature to increase rapidly within a few seconds when directly irradiated [28].

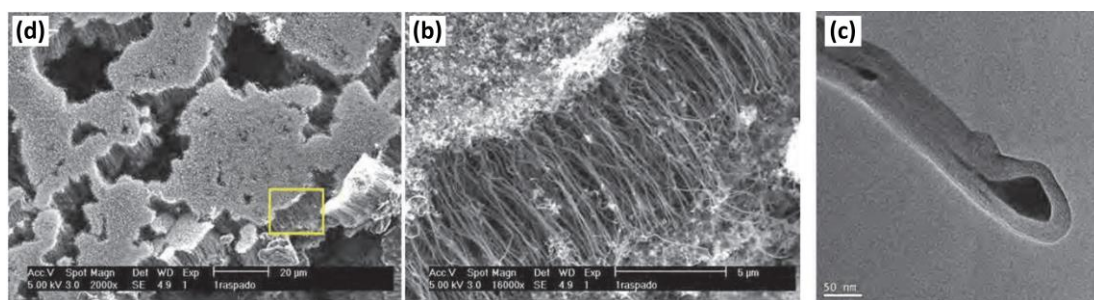


Figure 2.4: Material obtained in an evacuated ampoule directly exposed to microwaves for 10 min: a) SEM image at low magnification of parallel arrays of aligned MWNTs; b) higher magnification of the rectangular of a MWNT zone marked in (a), and (c) TEM of metal particle at the tip [28].

Yoon et al. [29] synthesized CNTs using activated carbon fibers (ACF) as carbon source. The activated carbon fibers were immersed in iron chloride solution, and placed in a quartz-tube. The solution was subjected to microwave irradiation treatment for 60 to 90 s at 400 W under the flow of argon. The MWCNTs covered the ACF surface with diameters of 10 to 40 nm. After only 30 s of irradiation, particles of a few tens of nanometers and large carbon particles were observed, while very thick fibrous carbon appeared after 120 s (Figure 2.5). In the absence of a catalyst, no CNTs were grown at similar conditions of reaction.

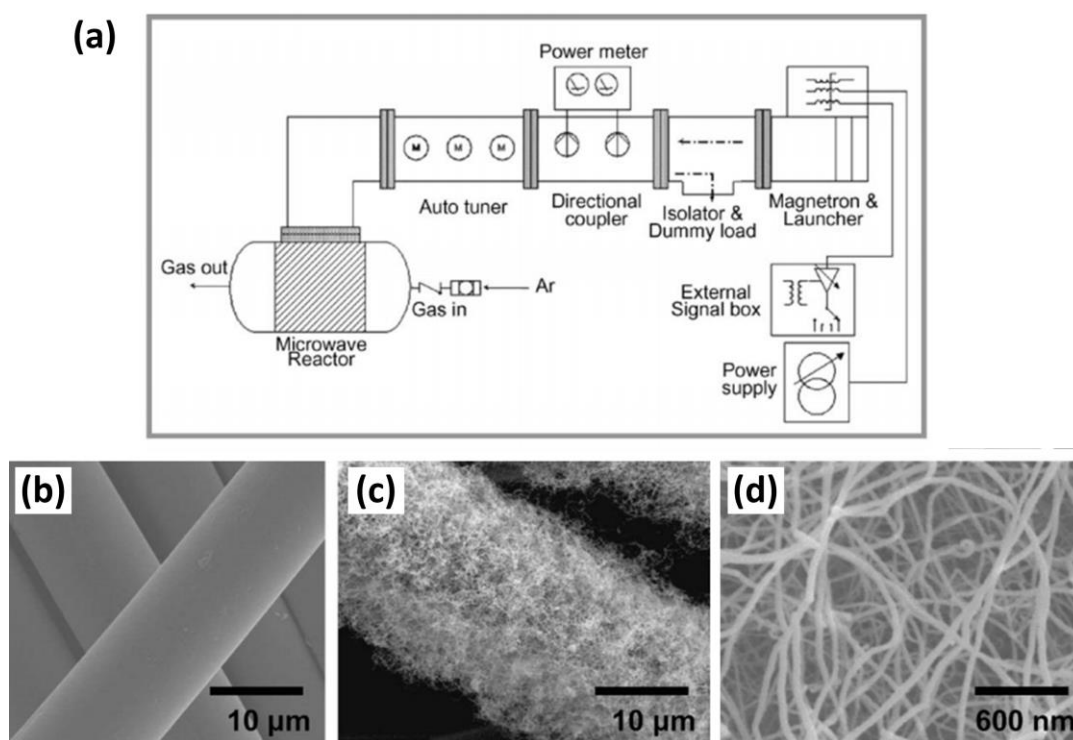


Figure 2.5: (a) Microwave irradiation system. Morphology of the ACF specimen (b) before microwave irradiation, (c) after microwave irradiation. (d) Magnified image of (b) [29].

The synthesis of CNT using impregnated graphite with nickel acetylacetonate was performed by Pentsak et al. [30]. The mixture was irradiated by means of a conventional MW oven for 5 to 30 min. The study analyzed the effects of gas

atmosphere on the catalyst with regards to the growth of CNTs. In this study, when the impregnated graphite was irradiated under vacuum conditions or under an inert atmosphere of argon the CNT was growth. Contrarily, no CNTs were formed under the oxygen atmosphere. The focus of this study was set on the influence of the surrounding atmosphere and was performed from the perspective of catalysis.

Takagi et al. [31] developed a method to synthesize CNTs at 800 °C from polystyrene by using a commercial MW oven equipped with a thermocouple and a thermal controller to regulate the temperature. The system comprises a microwave and a furnace coated with silicon carbide placed in the microwave oven cavity. The furnace temperature reached 800 °C after 5 minutes of microwave irradiation at 600 W power. Nickel nanoparticles and granular polystyrene were blended in a quartz glass tube placed in the furnace and irradiation for 10 min under a flow of nitrogen gas. The resulting CNTs have a diameter of 25 to 100 nm (Figure 2.6). The ideal concentration of nickel was found to be 30%, and the product-to-precursor ratio strongly correlated with increasing volume of precursors. Other verified carbon sources such as poly(vinyl alcohol) resulted in a very small yield, sugars yielded no CNTs, while a reasonably high amount of CNTs was realized with polyethylene [31].

In the PopTube approach [8, 32], catalyst powder was mixed with conductive materials such as conducting polymers, indium tin oxide and carbon fiber. The irradiation of the conductive material with MW rapidly increased the temperatures. As a result, the ferrocene was transformed to iron and cyclopentadienyl via pyrolysis, which can serve as a catalyst and a carbon source respectively (Figure 2.7a and b). The duration of the initiated synthesis took 15 to 30 s. Regrettably, no detailed information regarding the properties of the used microwave oven and the heating method was provided.



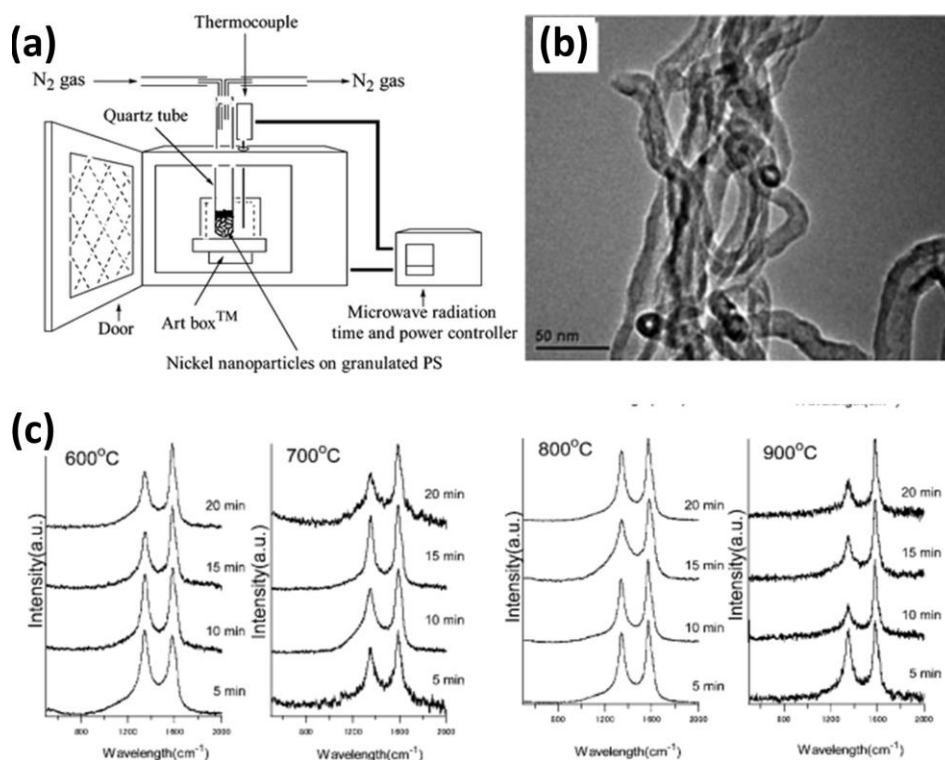


Figure 2.6: (a) Setup for synthesis of carbon nanotubes by using a remodeled domestic microwave oven and an Art Box, (b)TEM images of the products calcined at 800 °C and (c) Raman spectra of the carbon products at 600 °C, 700 °C, 800 °C and 900 °C for 5, 10, 15 and 20 min [31].

Hu et al. [ 86 ] used the PopTube approach and synthesized micrometer-long CNTs on an ultralight graphene aerogel without an additional carbon source. The ferrocene coating was applied by impregnation and, after drying, the sample was heated with a MW oven at 800 W for 1 min in a quartz tube flushed with argon [33].

Nie et al. [34] also used the ferrocene as a carbon source and a catalyst material in the synthesis of CNTs. A singular carbon fiber (3 to 4 cm long) was applied as a pyrolysis activator for the ferrocene in a closed glass flask. 100 mg of the ferrocene was irradiated using a commercial microwave for a duration of 20 seconds at 1000 W power to yield 40% of MWCNTs with an average diameter of approximately 20 nm (Figure 2.7c and d). The alternative use 1 mg commercial CNTs in place of carbon fibers as a microwave absorber also increased the amount of synthesized CNTs [34].

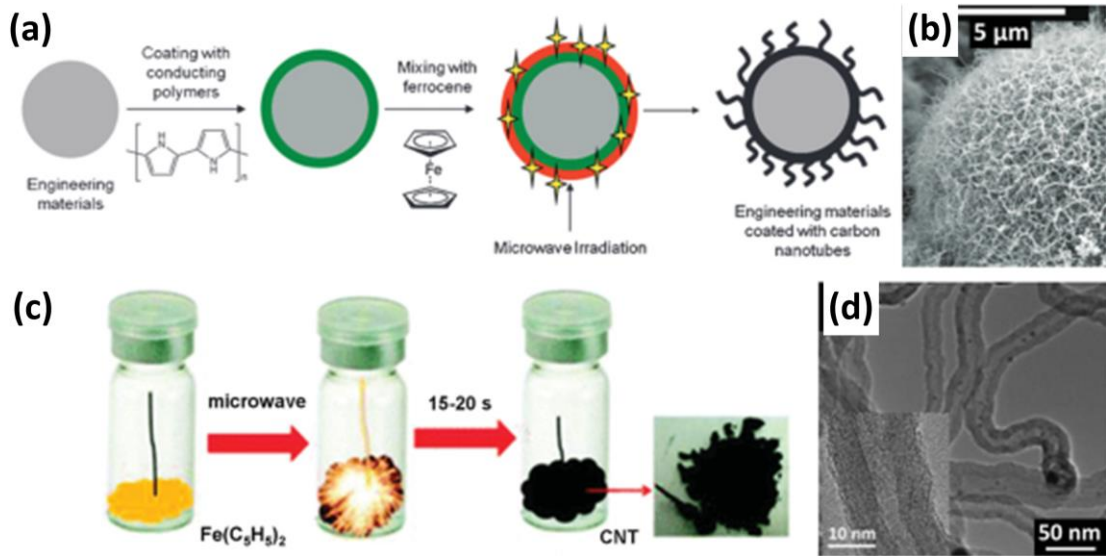


Figure 2.7: (a) Schematic illustration of CNT-fabrication processes utilizing solid precursors and additional susceptor materials, (b) Pop-tube approach applying a conducting polymer as MW susceptor to grow CNTs on engineering materials (b) FESEM images of the resulting (a) [8]. (c) Microwave synthesis triggered by a single carbon fiber vertically placed to ferrocene precursor powder resulting in MWCNTs and (d) TEM images of the resulting (c) [34].

Kure et al. [35] produced carbon nanotubes (CNTs) from plasma catalytic decomposition of polyethylene as a carbon source using a commercial microwave oven at 600 W and 2.45 GHz. Polyethylene and silicon substrate coated with iron (III) nitrate as a catalyst was placed in the reaction chamber to form the carbon nanotube. The CNTs were produced at 750°C during 1 hr and under atmospheric pressure of 0.81 mbar.

Another method with solid materials is the direct transformation of electrically conductive polymer structures into graphitic carbon nanostructures. Zhang and Liu firstly reported such an approach in 2006 [ 89 ]. The transformation was performed in air, using a domestic MW oven and irradiation times of 3 to 5 min. The main idea is that the conducting polymer nanostructure absorb microwaves radiation very efficiently, as a result, when subjected to microwave radiation, are rapidly carbonized

to nano carbons within one reaction step [36]. Table 2.1 summarizes the various types of CNT nanostructures synthesized by microwave irradiation.

Table 2.1: Summary of the CNT synthesized using microwave method.

Microwave oven setting		substrate	Precursor/chemical			CNT Morphology Characteristic		Raman peaks ratio $I_D/I_G$	Reference
Power (W)	Duration (min.)		Carbon base	Additive	Catalyst	Diameter (nm)	Length ( $\mu\text{m}$ )		
800	0.5-15	SiO <sub>2</sub> , Teflon, black carbon	C <sub>2</sub> H <sub>2</sub>	H <sub>2</sub> S	Co	50	-	1.8	[23]
600	30	-	CH <sub>4</sub>	C felt	-	40-120	-	0.92	[24]
300	5	Si	C <sub>2</sub> H <sub>6</sub> O	-	Fe, Co, Ni	50	-	-	[25]
700	10	-	TErGO	-	Ni(C <sub>5</sub> H <sub>5</sub> ) <sub>2</sub>	-	-	0.58	[26]
600	60	Si	PE	-	Iron nitrate	1-25	0.85	0.98	[35]
800	60-90	-	Gr	Sucrose, boric acid	-	50-400	1000-10000	-	[27]
700	10	-	Gr	Ferrous acetate	Fe(CO <sub>2</sub> C H <sub>3</sub> ) <sub>2</sub>	40-60	7-10	0.94	[28]
400	1.5	-	ACF	NH <sub>2</sub> .OH. HCl	FeCl <sub>3</sub> .6H <sub>2</sub> O	10-40	-	0.41	[29]
-	10-60	-	Gr	Ar	Ni, Co	7-40	0.1-0.6	-	[30]
600	10	-	PS	N	Ni	25-100	2	0.83	[31]
1250	0.25-0.33	ITO, glass, CF	PPy	Hexane	Fr, Fe(Co) <sub>2</sub>	6-15	-	-	[32]
-	0.25-0.5	-	Fr	CF		20	-	1.1	[34]

### 2.3 Gas sensor based on CNT

Hydrogen sensors devices can detect hydrogen gas molecules by generating an electrical signal with a value proportional to the concentration of hydrogen gas. Commercially, there are numerous and diverse kinds of hydrogen sensors. Over time, most of the hydrogen sensing principles have been studied and Recent development in fabrication techniques of nanomaterials had greatly improved the gas sensors performance. There a number of ongoing studies to improve the responsivity, selectivity, response time and accuracy of hydrogen sensors, in addition to reducing cost, sensor size and power consumption in order to meet the future requirements of a hydrogen economy [37, 38].

Jung et al. [39] reported the fabrication of gas sensors using multi-walled carbon nanotube (MWCNT) sheets on glass substrate. The fabricated sensors revealed a sensitivity of approximately 13% under 18000 ppm of H<sub>2</sub> gas at room temperature, with a response time of 20 s. It was found that a greater flow of gas carriers (2000 sccm) and higher thermal annealing temperature (100 °C) can increase the recovery response (Figure 2.8). Low and incomplete recovery of original resistance values after halting operating target gases is a drawback to using CNTs in the gas sensors. This is attributable to high binding energy and robust interactions between H<sub>2</sub> gas and CNTs.

Dhell et al. [40] fabricated a H<sub>2</sub> sensor based on functionalized multiwall carbon nanotube (F-CNTs) using H<sub>2</sub>SO<sub>4</sub> (10 M), HNO<sub>3</sub> (11 M) and H<sub>2</sub>O<sub>2</sub> (8.8 M) acid. The study attained relative sensitivities of approximately 0.9, 0.13 and 0.14% for 500, 3500, and 5000 ppm of H<sub>2</sub> gas, respectively, after 7 min of exposure. The recovery time of these sensors was found to be 95 s. F-MWCNTs exhibited a comparably higher response to H<sub>2</sub> gas than pristine multiwalled carbon nanotubes (P-MWCNTs). Using the Raman spectra, the crystallite size of 15.2 was achieved for the functionalized

nanotubes, while the crystallite size of P-MWCNTs decreases to 14.6 nm. The interplanar size of F-MWCNTs increased because of the attachment of functional groups to the surface of nanotubes. It is also observed that the recovery time decreases from the 190 s for pristine MWCNTs sensor to 100 s for the functionalized MWCNTs when exposed to 500 ppm of H<sub>2</sub> gas concentration (Figure 2.9). The dissociation of H<sub>2</sub> gas molecules to H atoms by the edges of functionalized MWCNTs accounts for the increase in sensing response of F-MWCNTs. These functional groups serve as catalytic sites for the dissociation of H<sub>2</sub> gas molecules.

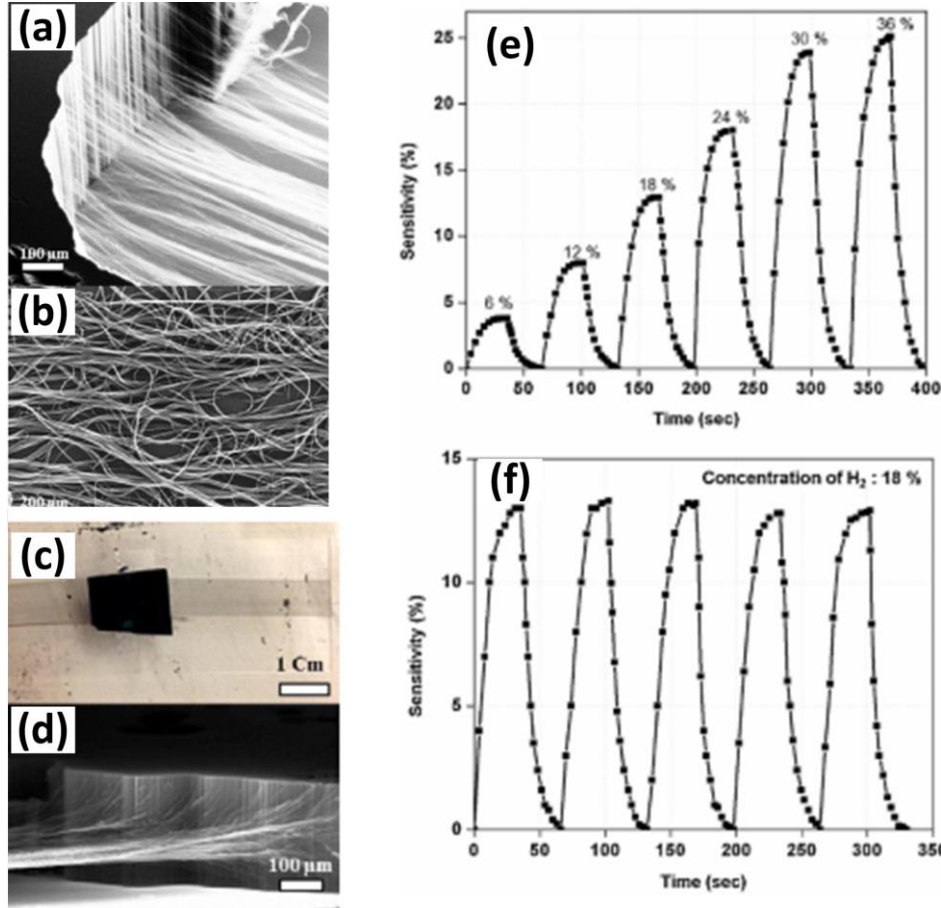


Figure 2.8: SEM images and a photograph of (a) spin-capable CNTs showing alignment of 430 μm MWCNTs, (b) morphology of the CNT sheets, (c and d) CNTs sheet pulling from the CNT forest, (e) Sensitivity and (f) cyclic response of the gas sensor after thermal annealing with 2000 sccm of N<sub>2</sub> [39].

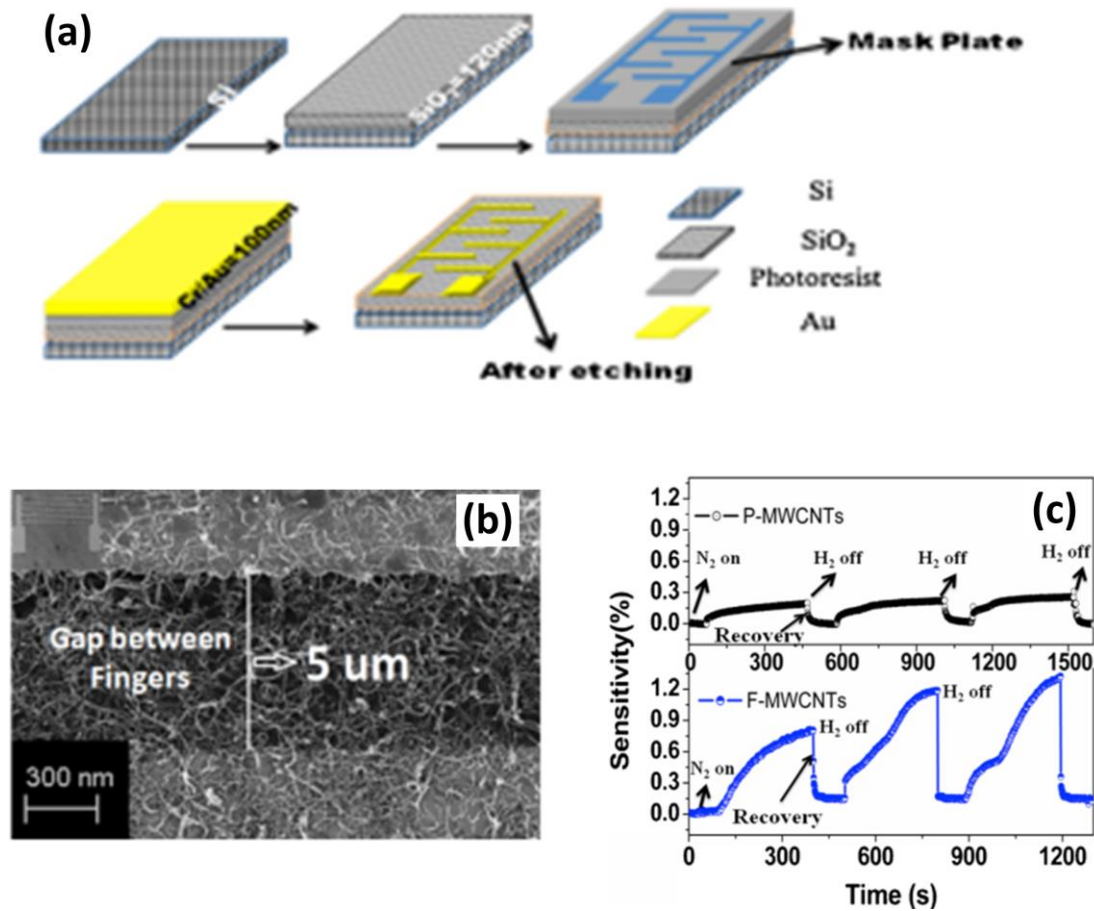


Figure 2.9: (a) Schematic diagram of fabricated device and (b) SEM image of fabricated interdigitated electrodes and (c) Sensor sensitivity of P-MWCNTs and F-MWCNTs film at different concentrations of H<sub>2</sub> [40].

Kong et al. [41] fabricated a room temperature H<sub>2</sub> gas sensors based on Pd functionalized SWCNTs via electron-beam evaporation deposition. In contrast to pure SWCNT bundles, the H<sub>2</sub> gas sensor was shown to be highly sensitive, up to 50% relative resistance, when exposed to 400 ppm H<sub>2</sub>. The response and recovery times were found to be 5–10 s and 400 s, respectively. It is proven that the Pd nanoparticles can split hydrogen molecules into separate atoms at room temperature, which dissolves into Pd and then reduces the work function of Pd. The electrons from Pd are subsequently transferred to SWCNT, resulting in increased resistance. Reversibly, the

dissolved atomic hydrogen in Pd can combine with O<sub>2</sub> in the air to form water and then exit the gas sensor, resulting in recovery of the sensor's original resistance.

Mubeen et al. utilized a simple electrochemical deposition method to fabricate a H<sub>2</sub> gas sensor [42]. At room temperature, the optimized sensor exhibited a resistance change of 0.42% per ppm for detected H<sub>2</sub> with a linear response of 1000 ppm. The recovery time varied with concentration, i.e. 20 minutes and 55 minutes for 100 ppm and 1000 ppm H<sub>2</sub>, respectively. Using a similar method, room temperature sensors were fabricated to detect H<sub>2</sub> on a flexible plastic substrate based on SWCNT functionalized with Pd nanoparticle. The sensors exhibited a relative response of 5% for 100 ppm H<sub>2</sub>. The response time for this sensor ranges from a few seconds up to a 5 minute to reach a saturation state. The response of ideal flexible sensors when exposed to 500 ppm H<sub>2</sub> is about 75%, while the response time for 10000 ppm H<sub>2</sub> at room temperature is approximately 3 seconds [43].

Ding et al. [44] fabricated H<sub>2</sub> gas sensor based on as-grown aligned CNTs in an anodic aluminum oxide (AAO) template. Using gold (Au) as an electrode in the absence of Pd, the CNTs sensor exhibited no response to H<sub>2</sub>. In contrast, the Pd-CNT sensor could detect H<sub>2</sub> from 1000 to 15000 ppm H<sub>2</sub> with response time of about 3-4 minutes. Similarly, nanoporous Pd film was utilized to develop sensors based on CNTs as-grown in an AAO template. The CNTs-supported Pd film sensor displayed a normal response time of less than 7 minutes for dilute H<sub>2</sub> (Figure 2.10). The Pd electrode CNT sensor exhibited less response time than CNT supported Pd film sensor, which is attributable to the stability of Pd film (non-peeling) even after exposure to H<sub>2</sub> gas. The Pd film contributes to the total resistance of the sensor based CNT-supported Pd film. Conversely, the Pd film and the CNTs both contribute to the total resistance of the Pd-electrode CNT sensor.

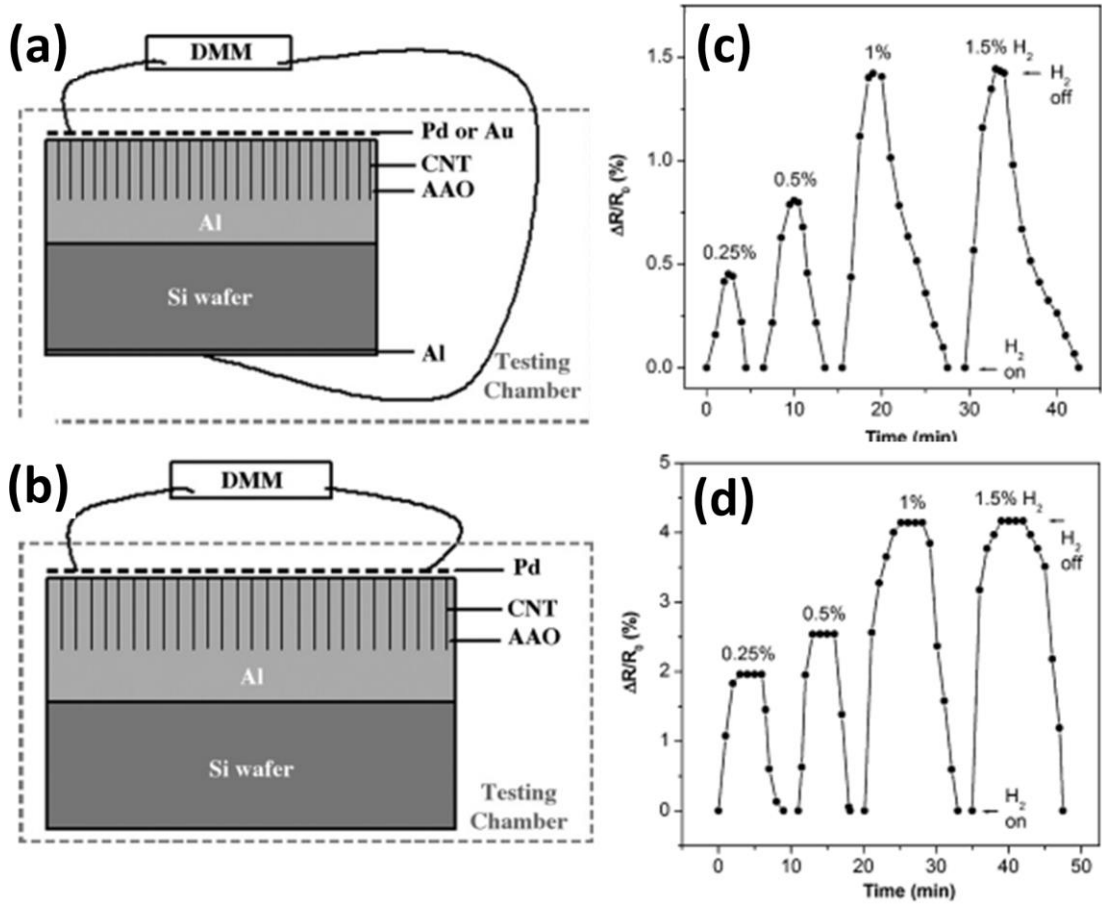


Figure 2.10: Resistive hydrogen sensors. (a) Metal-electrode CNT sensor, and (b) CNT-supported Pd film sensor. (c) Response of the Pd-electrode CNT sensor at medium H<sub>2</sub> concentrations and (d) Response of the CNT-supported Pd film sensor at medium H<sub>2</sub> concentrations [44].

Oakley et al. employed a filtration process to prepare SWCNTs films, subsequently coated with palladium [45]. The sensor based Pd-coated SWCNTs film detected H<sub>2</sub> at room temperature with sensitivities of 20% and 40% for 100 ppm and 500 ppm H<sub>2</sub>, respectively. The recovery time of the device when exposed to air was found to be approximately 30 s with power consumption of 25 mW (Figure 2.11).

In a different study, Junya et al., [46] used the dielectrophoresis method (DEP) to fabricate carbon nanotube (CNT) based gas sensor. A benefit of the DEP technique is its ability to generate contact between CNT and electrode and between CNT and other materials. However, the catalytic Pd surface can dissociate H<sub>2</sub> molecules into H



atoms, resulting in the reduction of CNT, which subsequently increases the resistance of the gas sensor. At 90 °C, the CNT sensors can detect 500 ppm H<sub>2</sub> in the air with recovery time of 600 s.

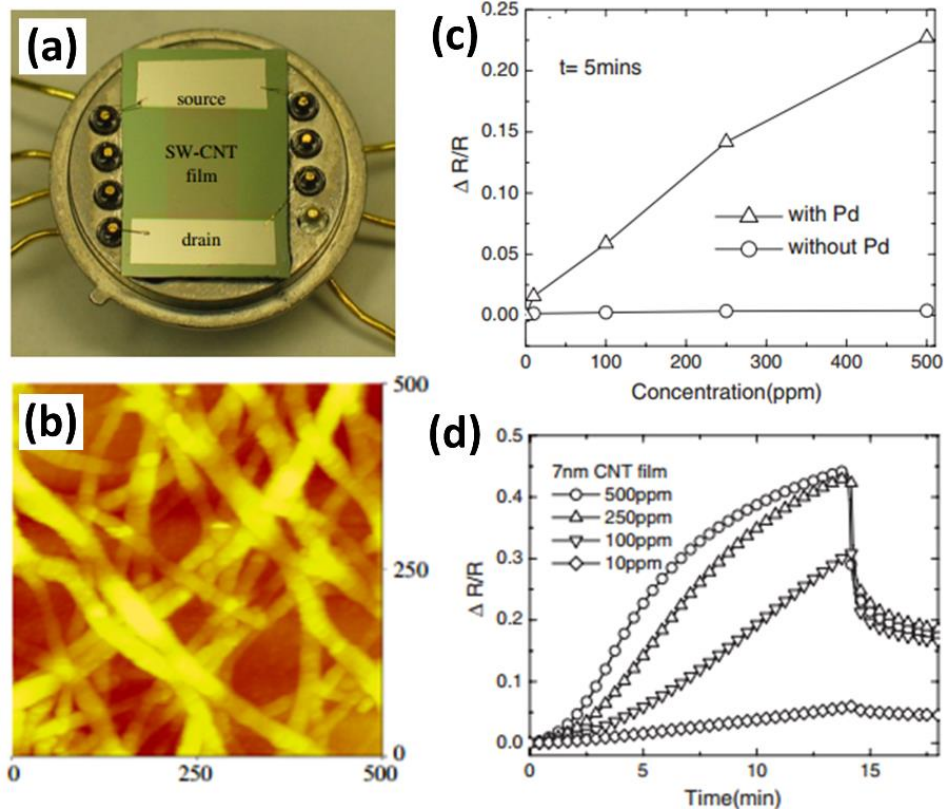


Figure 2.11: (a) Photograph of a gas sensor device, wired for testing. SWCNT films were 3 mm wide, and 6 mm long between source and drain pads. (b) Images of nominally 7 nm films with sputtered Pd (AFM, scale in nm). (c) Fractional change in resistance as a function of H<sub>2</sub> concentration in N<sub>2</sub>, the resistance was taken 5 min after exposure to the H<sub>2</sub>-containing ambient. (d)  $\Delta R/R$  as a function of time for exposure and recovery to the H<sub>2</sub> concentrations for 7 nm SWCNT films coated with sputtered Pd, recovery in N<sub>2</sub> [45].

Wang et al. suggested application of nanorods as hydrogen sensors [47]. ZnO nanorods were characterized towards hydrogen at room temperature. This study reported the response of bare ZnO and Pd coated ZnO nanorods. The deposition was conducted over a glass substrate with pre-existing Au contacts, and Pd deposition was performed with sputtering. The resulted nanorods covered 70% with a root mean

square (rms) roughness of 8 nm, and a catalytic effect was obtained (Figure 2.12). A strong increase in response to hydrogen was measured, especially at low concentration levels. Furthermore, no response to oxygen variations have been registered at room temperature; recovery time transients were faster than 20 s upon removal of H<sub>2</sub>.

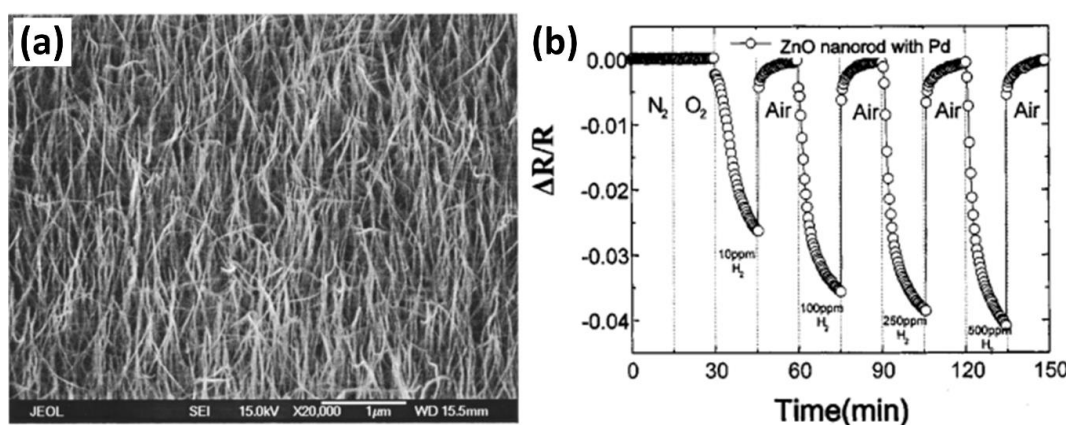


Figure 2.12: (a) Scanning electron micrograph of ZnO multiple nanorods and (b) relative response of Pd-coated nanorods as a function of H<sub>2</sub> concentration in N<sub>2</sub> [47].

Kadhim et al. [48] fabricated a metal–semiconductor–metal gas sensor using nanocrystalline SnO<sub>2</sub> thin film and palladium (Pd) metal. Ohmic barrier contact was formed without addition of glycerin, while Schottky contact was formed by adding glycerin. The room temperature sensitivity for hydrogen (H<sub>2</sub>) was 120 % in 1000 ppm H<sub>2</sub>, and the power consumption was 65 W, with response and recovery time of 214 s and 52 s respectively.

In the past years, numerous of synthesis techniques have grown rapidly. A variety of nanostructured materials with different morphologies have been successfully synthesized during last two decades, as summarized in the Table 2.2.